A Robust Real-Time 100G Transceiver With Soft-Decision Forward Error Correction [Invited]

Lynn E. Nelson, Guodong Zhang, Martin Birk, Craig Skolnick, Rejoy Isaac, Y. Pan, Christian Rasmussen, Graeme Pendock, and Benny Mikkelsen

***Abstract*—We demonstrate a 120 Gb/s coherent polarization-multiplexed quadrature-phase-shift-keyed transceiver with soft-decision forward-error-correction (SD-FEC) coding based on Turbo Product Code. This industry-first transceiver module utilizes a 40 nm complementary metal-oxide semiconductor (CMOS) application-specific integrated circuit with integrated analog-to-digital conversion, digital signal processing and SD-FEC, and is packaged according to a multi-source agreement from the Optical Internetworking Forum. Through several long-haul and ultra-long-haul system experiments (over 1000 km to 3760 km), we validate the robustness of the transceiver and demonstrate its high tolerance to various system impairments, including fiber nonlinearity, chromatic dispersion up to 60,000 ps/nm, polarization mode dispersion, polarization-dependent loss, polarization transients and multiple-path interference.**

***Index Terms*—Error correction codes; Optical fiber communication; Optical modulation; Optical receivers; Optical transmitter.**

I. Introduction

Research experiments in 2007 first demonstrated the polarization-multiplexed quadrature-phase-shift-keyed (PM-QPSK) modulation format with digital coherent reception at 100 Gb/s line rates and proved the practicality of 2 bit/s/Hz spectral efficiency in long-haul applications [1,2]. Intense further research and development followed, with the announcement in mid-2010 of the first commercial long-haul systems with 100G transponders utilizing a single carrier [3]. Current 100G systems are based on hard-decision forward error correction (FEC) and have ~1500 km reach over standard single-mode fiber (SSMF), where the transponders employ second-generation FEC codes with as high as 9.5 dB of net coding gain at 6.7% overhead [4]. However, there are applications where ultra-long-haul distances or similar reach over more challenging fibers are required. For these types of application, the third generation of FEC, soft-input–soft-output iterative decoding, i.e., soft-decision (SD) FEC [4–8], with higher coding gain has the potential to increase system margin for 100G by improving the transponder's optical-signal-to-noise-ratio (OSNR) sensitivity.

Various approaches have been proposed for SD-FEC, including Block Turbo Code based on Bose–Chaudhuri–Hocquenghem (BCH) product code [5], Turbo Product Code (TPC) based on two BCH codes [6] and triple-concatenated FEC based on soft-decision low-density parity-check (SD-LDPC) codes [7,8]. A recent paper reported the first real-time 120 Gb/s PM-QPSK industry-compliant transceiver module with integrated SD-FEC based on TPC and characterized its dense wavelength division multiplexing (DWDM) transmission performance [9]. The transceiver was then utilized in a commercial ultra-long-haul transmission system with reconfigurable optical add–drop multiplexers and neighboring 40 Gb/s channels [10]. In this follow-up paper we provide further details on the performance of the 120 Gb/s transceiver including its tolerance to various linear and nonlinear transmission impairments.

The paper is organized as follows. In Section II, the real-time, 120 Gb/s, PM-QPSK transceiver is described, including its back-to-back performance. Section III summarizes measurements exploring the transceiver's tolerance to nonlinearities from adjacent 100G and 40G channels in wavelength-division-multiplexed systems. Section IV describes the transceiver's tolerance to multiple-path interference (MPI), while Section V reports the transceiver's tolerance to polarization mode dispersion (PMD), polarization-dependent loss (PDL), and polarization transients in a 10 × 100 km transmission experiment. In Section VI, we review the transceiver's performance in an ultra-long, 3760 km transmission system, to our knowledge the longest reach reported for a 100G real-time transceiver in terrestrial, commercial systems with 40G neighbors and reconfigurable add–drop multiplexers (ROADMs). Finally, in Section VII we summarize our results.

II. 120 Gb/s PM-QPSK Transceiver

The coherent PM-QPSK transceiver is implemented in a 5×7 inch^2 multi-source-agreement (MSA) package, designed to be consistent with recommendations from the Optical Internetworking Forum (OIF). Figure 1(a) shows a block diagram of the MSA transceiver, which contains a state-of-the-art 40 nm complementary metal-oxide semiconductor (CMOS) application-specific integrated circuit (ASIC). On the receive

Manuscript received July 20, 2012; revised September 21, 2012; accepted September 21, 2012; published October 29, 2012 (Doc. ID 173044).

Lynn E. Nelson (e-mail: lenelson@research.att.com), Guodong Zhang, Martin Birk, Craig Skolnick, and Rejoy Isaac are with AT&T Labs, Middletown, New Jersey 07748, USA.

Y. Pan, Christian Rasmussen, Graeme Pendock, and Benny Mikkelsen are with Acacia Communications Inc., Maynard, Massachusetts 01754, USA.

Digital Object Identifier 10.1364/JOCN.4.00B131

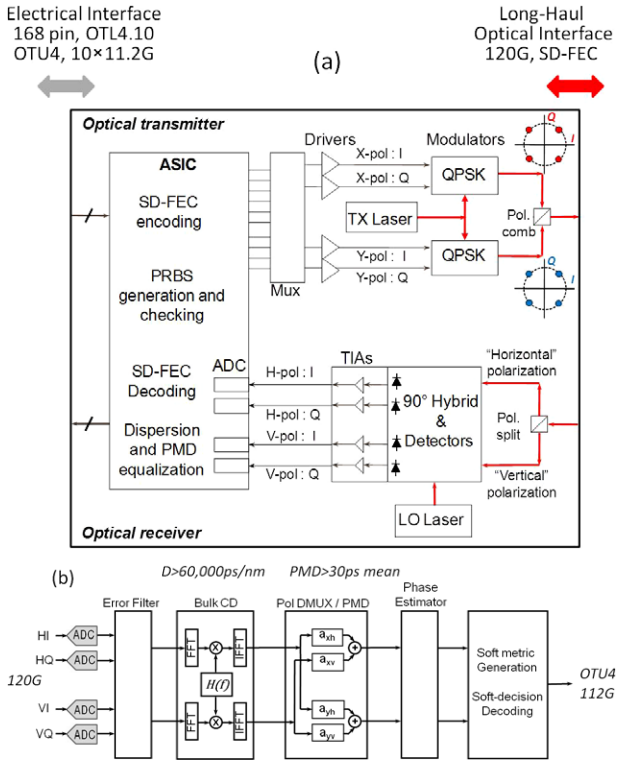

Fig. 1. (Color online) (a) Block diagram of the 100G MSA transceiver. (b) Block diagram of digital signal processing in the receiver.

side, four eight-bit, 63 Gsamples/s analog-to-digital converters (ADCs) are followed by the digital signal processing (DSP) engine, shown in Fig. 1(b). The DSP performs chromatic dispersion (CD) compensation of up to 60,000 ps/nm via frequency domain equalization [11] and PMD compensation of up to 30 ps mean PMD via a time-domain butterfly structure, which uses fractional tap spacing, where the tap updates are based on the constant modulus algorithm. The response time of the equalizer is of the order of microseconds. The phase estimation for carrier recovery [12] utilizes a feedforward method and averages over an adjustable block size. For the measurements reported in this paper, a block size of 32 symbols was generally used for the carrier phase estimation.

In addition, the ASIC performs the SD-FEC encoding on the transmit side and the corresponding SD-FEC decoding on the receive side. The SD-FEC is based on a TPC that is designed to convert a 1.9×10^{-2} pre-FEC bit error ratio (BER) to less than 1×10^{-15} after decoding, corresponding to an 11.1 dB net coding gain. The coding gain is achieved with an overhead of 15%, resulting in a line rate of 120 Gb/s from the MSA transceiver. Several TPC blocks are interleaved to tolerate bursts of more than 2000 errors. The TPC is well suited for very high-data-rate applications, because rows and columns can be independently decoded, enabling a parallelized implementation. Unlike LDPC-based FECs, which are known to have error floors at relatively high BER [8], the implemented TPC has no error floor. (The post-BER curve is predicted to have a flaring below 1×10^{-20}.)

In addition to the ASIC, the transmitter consists of a high-power, tunable, narrow-linewidth laser and a lithium niobate ($LiNbO_3$) quad-parallel-Mach–Zehnder (QPMZ) modulator to generate the PM-QPSK signal. The QPMZ modulator is driven with four 30 Gb/s data streams generated by multiplexing the lower-speed SD-FEC-encoded data streams provided by the ASIC. The optical receiver is comprised of a coherent mixer and an integrated balanced front-end with linear trans-impedance amplifiers (TIAs) and automatic gain control. A second narrow-linewidth tunable laser is used as the local oscillator in the receiver.

In order to provide full optical/electrical test functionality, the 100G transceiver module is mounted on an evaluation card, designed to interface with an ACTA compliant rack or to be used stand-alone. The "100G line card" includes a socket for a 100G CFP for the received and transmitted client signals, and the CFP and MSA transceiver are electrically connected via an optical channel transport lane protocol 4.10 (OTL4.10) interface. The MSA transceiver can either transmit the received optical channel transport unit 4 (OTU4) client signal after adding SD-FEC encoding or it can internally generate an OTU4-framed pseudo-random bit sequence and subsequently encode SD-FEC. On the receive side, the MSA transceiver can perform error checking on the PRBS payload or decode the OTU4 client signal from the received line-side signal and forward the client signal to the 100G CFP for subsequent transmission to the 100G OTU4 test set. In both cases, the MSA transceiver can report typical FEC statistics, such as the pre-FEC BER and if any post-FEC uncorrected blocks are present. A 100G JDSU test set has been used to verify the BER accuracy of the MSA transceiver. For the results reported in this paper, when the 100G client was not available, an OTU4-framed PRBS of $2^{31} - 1$ generated by the 100G transceiver was used, and the pre-FEC BER average and post-FEC error count over 10 s intervals were read from the transceiver. In back-to-back, the required OSNR for 1.9×10^{-2} BER is 12.0 dB/0.1 nm.

III. Nonlinear Tolerance

The 100G transceiver performance has been measured in two separate long-haul DWDM transmission systems, the first with 100 Gb/s neighboring channels [9] and the second with 40 Gb/s neighbors [10]. These experiments were designed to test the tolerance of the transceiver and its FEC threshold to single-channel and multiple-channel nonlinearities occurring in G.652 SSMF systems.

A. 100 Gb/s 1000 km System

Figure 2 shows the 100 Gb/s system, where test-bed transmitters generate two sets of 100-GHz-spaced PM-QPSK channels via bulk modulation at 28 Gbaud. After combining the loading channels with the test channel from the 100G transceiver via a 50 GHz commercial wavelength-selective switch (WSS), there were 40 WDM channels at 50 GHz spacing, as shown by the inset in Fig. 2. The test-channel wavelength was chosen to be 1552.52 nm, which was approximately at the center of the wavelength band. The signals were transmitted through ten spans of 100 km of SSMF, each having an average loss of 20.5 dB. No optical compensation for CD or PMD was

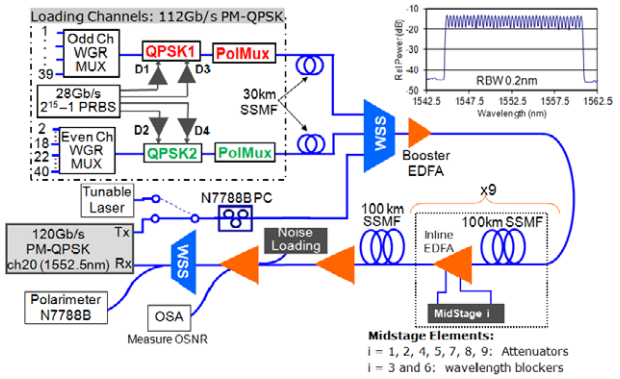

Fig. 2. (Color online) Block diagram of the 100 Gb/s WDM test setup over the uncompensated 1000 km link. The tunable laser, N7788B polarization controller (PC) and polarimeter were added for the experiments of Section V. Inset: the 40-channel spectrum at the booster output.

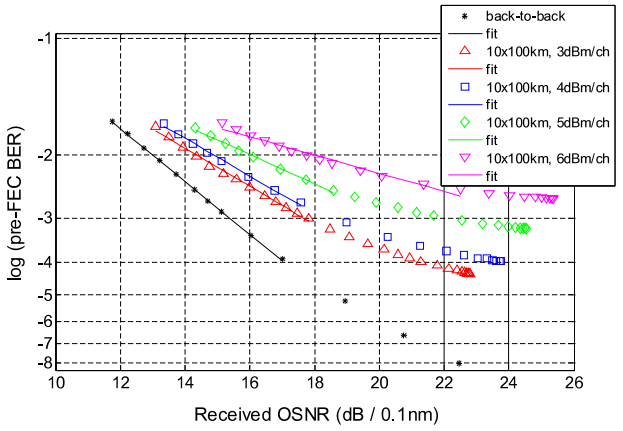

Fig. 3. (Color online) Measurements of pre-FEC BER versus OSNR for the 100 Gb/s MSA transceiver as channel 20 of the 40 × 100 Gb/s 1000 km system, with +3 to +6 dBm/ch launch powers into the spans.

used in the link; hence, the MSA transceiver compensated for approximately 17,000 ps/nm of chromatic dispersion. After each span, a two-stage erbium-doped fiber amplifier (EDFA) was used to amplify the optical signal power. To optimize the gain tilt, variable optical attenuators were introduced at the mid-stages of EDFAs 1, 2, 4, 5, 7, 8, and 9, while 50 GHz grid wavelength blockers at the mid-stages of EDFAs 3 and 6 allowed per-channel equalization. The total launch power into each span could be varied from +19 to +21 dBm, while still maintaining a flat channel spectrum to within ±1.5 dB at the input to each span. Following the tenth fiber span, the test channel was noise loaded, and its OSNR was measured with an optical spectrum analyzer (OSA). Finally, a second commercial 50 GHz WSS was used to de-multiplex the test channel before it was sent to the receiver input of the 100G transceiver.

Figure 3 presents BER curves after 1000 km WDM transmission for launch powers of +3, +4, +5 and +6 dBm/channel into the fiber spans. (To reach +6 dBm/ch, 20 channels in the center of the band were transmitted.) At +3 dBm/ch, the OSNR

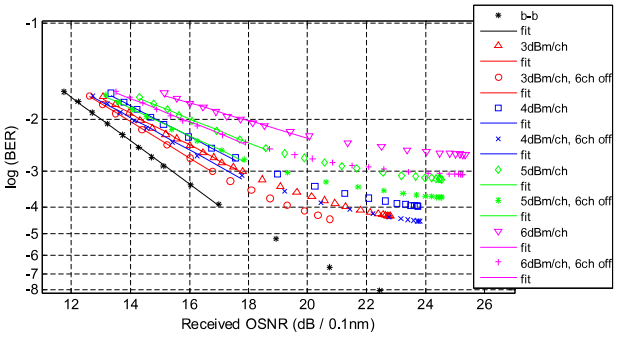

Fig. 4. (Color online) Comparison of the measured pre-FEC BER versus OSNR curves from Fig. 3 with the curves measured when the three channels on both sides of channel 20 were turned off.

penalty relative to back-to-back is 1.0 dB for a BER of 1.9×10^{-2} (the SD-FEC threshold). Moreover, the received OSNR after 1000 km is 22.8 dB, indicating that sufficient margin remains for transmission distances of 2000 km. As shown in Fig. 3, the OSNR penalty increases to 3 dB for +6 dBm/ch; however, at that launch power, the BER floor is still well below the FEC threshold. To test the impact of the neighboring 100G channels, BER curves were also measured at the different launch powers when the six nearest neighbors (i.e., ch 17–19 and 21–23) were turned off. To maintain the same per-channel power and EDFA loading, three additional channels were turned on at the short and long wavelength ends of the spectrum. Figure 4 shows a comparison of the BER curves for the channel under test with neighboring 50-GHz-spaced, 100G channels and with nearest neighbors spaced 200 GHz from the channel under test (i.e., with ch 17–19 and 21–23 turned off). At +3 dBm/ch, the required OSNR difference is only 0.3 dB, while the difference is 1.5 dB for +6 dBm/ch. Note that, given the SSMF dispersion and the uncompensated link, we believe the 2 Gbaud lower symbol rate of the loading channels compared with that of the channel under test will have only a minor impact on the measured WDM penalties. In fact, the 28 Gbaud loading channels walk through the channel under test at a slightly slower rate than 30 Gbaud loading channels would, and thus the measured WDM penalties may be slightly higher than the actual WDM penalties would be with loading channels at the same 30 Gbaud symbol rate as the channel under test.

As mentioned previously, the SD-FEC has been designed to convert a pre-FEC BER of 1.9×10^{-2} to less than 1×10^{-15} after SD-FEC decoding, corresponding to more than 11 dB net coding gain. In the experiments, the measured FEC threshold is in good agreement with prediction. Figure 5 presents the recorded post-FEC errors after SD-FEC decoding as a function of measured pre-FEC BER for the different launch powers, including the points from the curves of Fig. 3. Comparing the curve for back-to-back with those after transmission verifies that the FEC threshold—and thereby the coding gain—is essentially maintained in the presence of fiber nonlinearities. The FEC threshold was measured to change by <0.15 dBQ at power levels up to +6 dBm per channel, the maximum launch power attainable in this setup. To test repeatability, BER curves for 3 dBm/ch and 5 dBm/ch were measured twice, with slightly different received OSNRs.

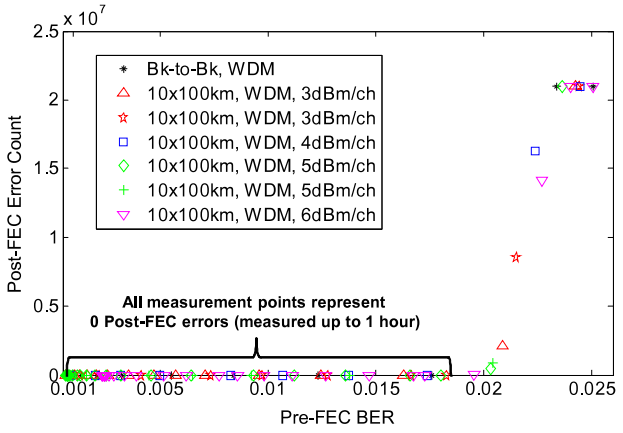

Fig. 5. (Color online) Post-FEC errors versus pre-FEC BER recorded before and after 1000 km transmission with different launch powers.

B. 40 Gb/s 1920 km System

Next, the 120 Gb/s transceiver was included as an alien wavelength in a 24 × 80 km commercial line system with 40G 50-GHz-spaced PM-QPSK neighboring channels. As shown in Fig. 6(a), the 100G channel at 194.2 THz (1543.73 nm) and six neighboring 40G PM-QPSK channels passed through five ROADMs that support 50 GHz channel spacing and include 1 × 9, liquid-crystal-on-silicon WSSs. After being dropped at ROADM5 after 1920 km, the 100G signal was either received by the OTU4 transponder or amplified and sent through system B (Fig. 6(b)), which will be discussed in Section VI. Both systems had 80 km spans of SSMF with average attenuation of 20 dB per span and low PMD (link design value 0.04 ps/km$^{1/2}$). The systems are optimized for coherent PM-QPSK 40G transmission with no optical dispersion compensation and utilize only EDFAs.

The performance dependence on launch power in the 1920 km system was studied by varying the 100G channel power from −4 to +2 dBm, while the 40G channel powers were maintained at −2 dBm/channel. As shown in Fig. 7(a), the 100G channel has the lowest pre-FEC BER at 0 dBm launch power. On the other hand, Fig. 7(a) shows that the 100G channel's impact on its neighboring 40G channels is relatively small over the 6 dB range. At optimum launch power of 0 dBm, the 100G channel has nearly negligible impact on the neighboring 40G channels. Next the launch powers of the 40G channels were varied, while maintaining the 100G channel power at the optimal 0 dBm. Figure 7(b) shows that the −2 dBm/channel is the optimum power for the 40G channels and that the 100G channel has significant tolerance to nonlinearities from the 40G WDM channels. As the launch power of 40G channels was increased from −6 dBm/ch to 0 dBm/ch, the pre-FEC BER for the 100G channel only degraded from 1.2×10^{-4} to 3.8×10^{-4}. In summary, for the 1920 km transmission, the optimum 100G launch power is about 2 dB higher than that for 40G, enabling 2 dB higher received OSNR for 100G compared with 40G.

IV. Tolerance to Multiple-Path Interference

Carrier networks are often comprised of various types and vintages of optical fiber and splices between cable sections. Older embedded fiber may have mechanical splices that exhibit high reflections, and/or it may have higher transmission loss, in which case the use of distributed Raman amplification may be utilized to bridge long spans. Multiple reflections along a transmission link or double Rayleigh scattering within a fiber amplifier cause time-delayed replicas of the signal to occur. These delayed signals beat with the signal at the receiver and cause the impairment known as MPI. Crosstalk in photonic devices can cause similar in-band, incoherent crosstalk. It is therefore important to understand the tolerance of 100G PM-QPSK signals to MPI, and in particular to verify that the SD-FEC performance is not significantly impacted by MPI.

In prior work, the impact of MPI has been studied at 10 Gb/s [13,14] for non-return-to-zero (NRZ), return-to-zero (RZ), phase-shaped-binary, and differential-phase-shift-keyed formats and at 40 Gb/s [15] for NRZ, RZ, and carrier-

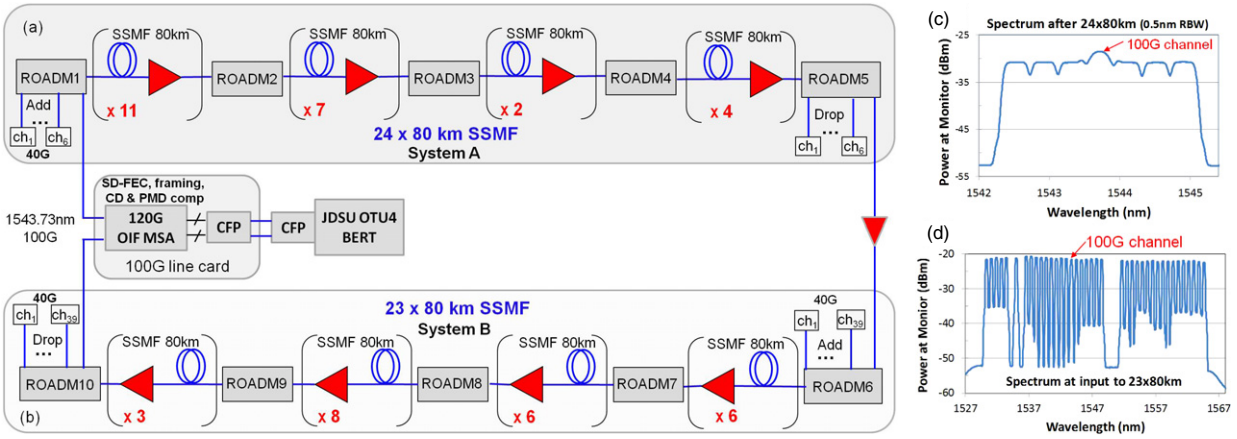

Fig. 6. (Color online) (a) Transmission system A and (b) transmission system B. Optical spectra (measured in 0.5 nm RBW) (c) after system A and (d) at the input to system B.

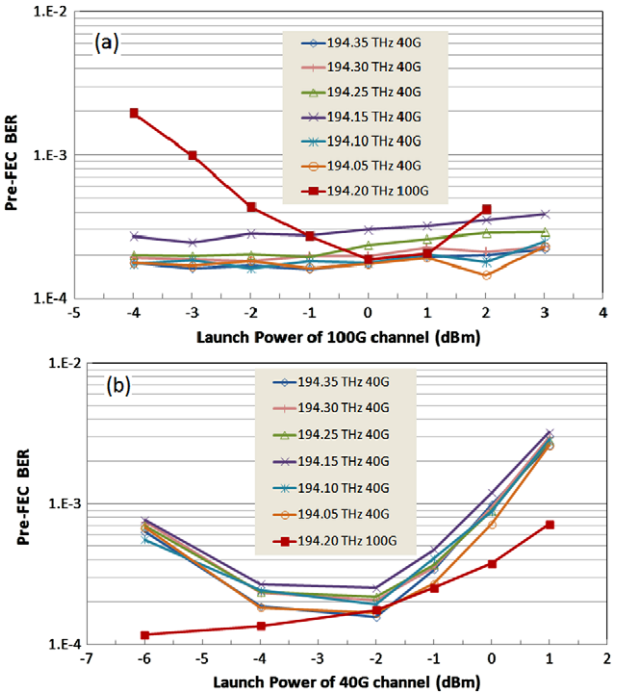

Fig. 7. (Color online) (a) Pre-FEC BER versus 100G launch power after 1920 km. (b) Pre-FEC BER versus 40G launch power after 1920 km.

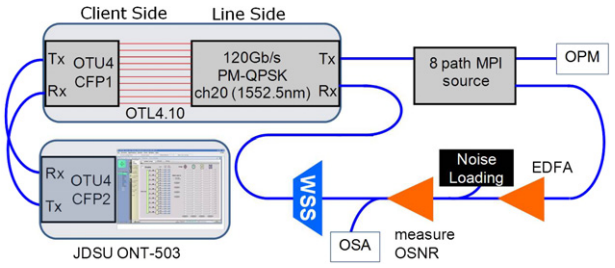

Fig. 8. (Color online) Schematic diagram of the setup for MPI tolerance tests. OPM: optical power meter.

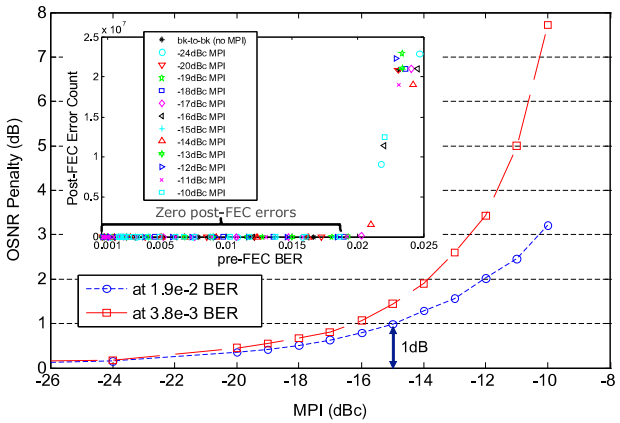

Fig. 9. (Color online) OSNR penalty as function of MPI at 1.9×10^{-2} and 3.8×10^{-3} pre-FEC BER. Inset: post-FEC error count versus pre-FEC BER recorded for different MPI levels.

suppressed RZ formats, all with direct detection. More recently, the MPI tolerance of a 40G PM-QPSK coherent transponder with HD-FEC and real-time DSP was reported in [16]. The polarization independence of the MPI-induced penalties was confirmed, as expected due to the fact that the PM-QPSK signal is essentially polarization scrambled, and a small advantage for coherent detection over direct detection was shown in the presence of low amplified spontaneous emission (ASE) noise [16].

Measurements of the impact of MPI on a 100 Gb/s coherent transponder were first reported in [9], where the 100G MSA transceiver with SD-FEC was evaluated using an MPI source that provides delayed signal replicas of equal power from eight paths. The eight paths represent pairs of reflections separated by distances of 2.5 km to 20 km, in steps of 2.5 km, to emulate MPI that could occur due to reflections at mechanical splices between cable sections. As shown in Fig. 8, the signal from the line-side transmitter was sent through the eight-path MPI source, and at the output, an optical power meter was utilized to monitor the signal power and MPI power in order to determine the crosstalk ratio. After the optical signal was combined with the MPI, the signal was ASE loaded for BER versus received OSNR measurements at the line side and interpolation of the induced penalty at a target BER.

BER curves were measured for MPI-to-signal power ratios from −24 dBc to −10 dBc and compared with the back-to-back case. Figure 9 plots the OSNR penalty as a function of MPI level. At 3.8×10^{-3} BER, approximately 1 dB of OSNR penalty was observed for −16 dBc of MPI, whereas the MSA transceiver tolerates −15 dBc of MPI with 1 dB of OSNR penalty at 1.9×10^{-2} BER. The inset of Fig. 9 plots the post-FEC error count versus the pre-FEC BER and shows that the SD-FEC threshold remained at the same pre-FEC BER for MPI as high as −10 dBc, thus indicating that noise from MPI is not degrading the SD-FEC performance.

In addition, a soak test was performed at −10 dBc MPI using a 100G client signal. As shown in Fig. 8, for these measurements, a JDSU ONT506 100G test set provided an OTU4 client signal to a 10 × 10G Santur CFP, which was connected to a second 10 × 10G CFP on the OTU4 transponder blade. ASE noise loading was added to degrade the pre-FEC BER to $\sim 1.35 \times 10^{-2}$, and the pre-FEC BER was recorded from the line side while the 100G performance was monitored with the client-side test set. As shown in Fig. 10, the pre-FEC BER was stable over the 24 hour soak with MPI, and zero errors were recorded on the external 100G test set at the client side.

V. Tolerance to Polarization Impairments

In coherent systems, relevant polarization effects include PMD, PDL and polarization transients. While the development of digital coherent receivers was driven first and foremost by the demand for higher spectral efficiency, a positive by-product of their development has been a significant increase in the tolerance of 40 Gb/s and 100 Gb/s signals to polarization impairments. As late as 2007, it was generally accepted

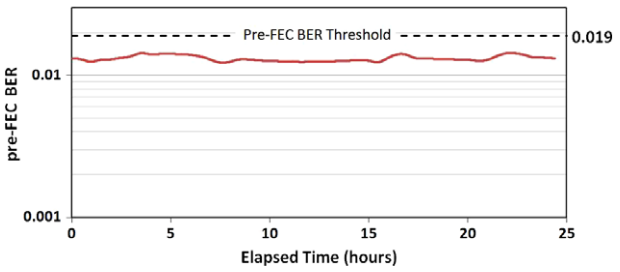

Fig. 10. (Color online) Soak test of MPI tolerance: line-side pre-FEC BER over 24 hours with MPI of −10 dBc and ASE noise loading. No errors were recorded on the client side.

that a 40 Gb/s DPSK signal could tolerate about 10 ps of differential group delay (DGD) with a receiver based on a delay line interferometer and differential detection [17]. However by 2008, 40 Gb/s PM-QPSK real-time coherent transponders demonstrated tolerance to instantaneous DGDs of more than 100 ps [18,19].

A. Polarization Mode Dispersion

In principle, CD and PMD of all orders can be compensated completely with a sufficiently complex electronic equalizer, since they are linear impairments. However, in practice, electronic equalizers can be implemented only with a limited number of taps, thus limiting the CD and PMD that can be effectively compensated. For example, calculated PMD-induced outage probabilities for PMD equalizers with various numbers of taps are shown in [20]. Recent measurements of real-time 40 Gb/s [18,19] and early 100 Gb/s coherent PM-QPSK transceivers [21,22] have elucidated the PMD tolerances that can be achieved, where in [22] an FPGA-based, real-time coherent receiver for a single-carrier 100 Gb/s PM-QPSK signal showed tolerance to more than 60 ps DGD.

The PMD tolerance of the 100G MSA transceiver with SD-FEC was evaluated using the setup shown in Fig. 2, where high PMD fibers and polarization-maintaining fiber (PMF) segments along with polarization controllers (PCs) replaced the attenuators at the EDFA mid-stages to distribute the PMD along the transmission path. Table I lists these PMD elements, where the overall mean DGD (over the C-band) is 50 ps. As shown in Fig. 2, an optical switch was used to replace the PM-QPSK signal with a tunable laser at the same wavelength, in order to characterize the PMD and PDL vectors over wavelength using an Agilent N7788B polarization controller at the system input to launch six polarization states and the N7788B polarimeter at the system output. Frequency steps of 2 GHz were utilized, and the PDL calculation is related to the Mueller–Stokes method [23] (using power only). The PMD measurement used a polarimetric method similar to the Mueller matrix method [24] and Jones matrix eigenanalysis [25]. Efforts were made to maintain a stable transmission path by securing all fiber jumpers and isolating the PMF and PMD spools from air currents and ambient temperature changes. For all the measurements of PMD and PDL tolerance reported in Section V, the launch power into the spans was +17 dBm for the 40 WDM channels (+1 dBm/ch). With no PMD inserted into the EDFA mid-stages, the required OSNR was 12.5 dB for a pre-FEC BER of 1.9×10^{-2}.

The procedure for measuring the 100G MSA transceiver's performance in the presence of PMD was as follows. First the PCs at the EDFA mid-stages 1, 2, and 5 were randomly set to change the PMD state of the transmission line. An estimate of the DGD was obtained from the 100G MSA transceiver by reading the coefficients in the equalizer, as in [26]. When the DGD estimate was greater than a chosen threshold (e.g., 50 ps), the tunable laser was switched through the 10 × 100 km transmission line and the PMD and PDL were measured. Then a BER versus received OSNR curve was measured for the 100G MSA transceiver. Finally, the PMD and PDL were measured again as a check of the system stability. During three different runs with DGD thresholds chosen at 25, 50, and 80 ps, a total of 3530 PMD states were generated, of which 265 states had sufficiently large DGD for BER measurement. Figure 11 displays, for these 265 states, the measured required OSNR for 1.9×10^{-2} pre-FEC BER versus the measured DGD (average of the DGD measured before and after the BER measurements). In these measurements, the launch state of polarization was fixed (i.e., not scrambled) and random relative to the PMD vector. The measured PDL was less than 0.8 dB for all PMD states. Figure 11 shows that, over the entire 25–100 ps range of DGDs obtained from our experimental setup, the performance of the 100G MSA transceiver is essentially flat and within 0.3 dB of the required OSNR with no PMD in the transmission line.

In addition, the DGD reported by the 100G MSA transceiver during the BER measurement was compared with the measured DGD. The inset of Fig. 11 shows a plot of the histogram of the differences between the DGD reported by the 100G transceiver and the measured DGD (average of DGDs measured before and after the BER curve). There is a systematic offset of −3.6 ps, which could be caused by a slight differential delay between the two polarizations within the transceivers. For this set of measurements, the monitor was always within 10.5 ps of the measured DGD value, and 93% of the monitor DGDs were within 8 ps of the measured DGD. The difference is partially due to the 3.6 ps systematic offset, while up to ~6 ps can be attributed to drift in the PMD of the transmission path during the time it took to make the measurements for a particular PMD state. For this limited statistical sample size, the histogram shows that the 100G MSA transceiver provides a reasonable estimate of the system DGD as measured by the Agilent apparatus. Such a DGD estimate could be used to track the PMD changes of a system over time, as in [27].

B. Polarization Dependent Loss

Although PMD can be effectively equalized, PDL is a more challenging impairment for coherent systems [28–31], particularly for those employing numerous ROADMs. Depending on the relative orientation of the polarization tributaries to the PDL axis, a single PDL element causes a power and/or OSNR difference of the two polarization tributaries and/or non-orthogonality of the (originally orthogonal) polarization tributaries. A polarization-multiplexed signal in a system with

TABLE I
ELEMENTS AT EDFA MID-STAGES FOR THE EXPERIMENTS DISCUSSED IN SECTION V

EDFA mid-stage	10 × 100 km with PMD (Subsection V.A)	10 × 100 km with PMD + PDL (Subsection V.B)
1	31.4 ps mean PMD + PC	31.4 ps mean PMD + PC
2	PMF 31 ps + PC	PMF 31 ps + PC
3	attenuator	3 dB PDL (with 6.5 ps DGD) + PC
4	wavelength blocker	wavelength blocker
5	8.5 ps mean PMD + PC	8.5 ps mean PMD + PC
6	18.6 ps PMF + PC	18.6 ps PMF + PC
7	wavelength blocker	wavelength blocker
8	attenuator	2 dB PDL + PC
9	9.5 ps PMF	9.5 ps PMF

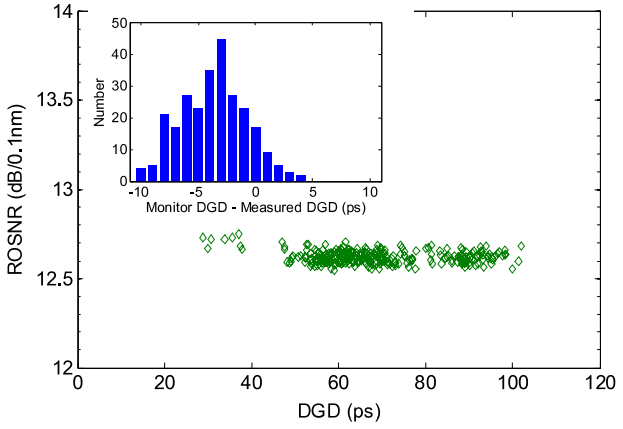

Fig. 11. (Color online) Measured required OSNR for 1.9×10^{-2} pre-FEC BER versus measured DGD of the 10 × 100 km transmission line with high PMD. Inset: histogram of differences between the monitor DGD (i.e., DGD value reported by the 100G MSA transceiver) and the measured DGD.

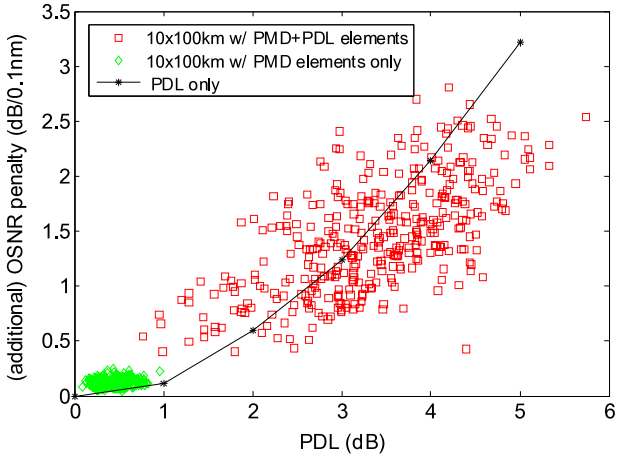

Fig. 12. (Color online) Measured additional OSNR penalty (defined in the text) versus PDL for the 10 × 100 km systems with PMD and PDL elements (red squares) and with PMD elements only (green diamonds). The black curve shows a separate measurement with first-order PDL only, where the OSNR penalty is the difference in required OSNR to have no uncorrectable FEC blocks with and without PDL.

multiple amplified spans and multiple, randomly oriented PDL elements will incur both impairments. DSP can effectively separate the tributaries even when they are no longer orthogonal, thus partially compensating PDL [18]; however, DSP is not able to compensate the degraded OSNR of one of the polarization tributaries.

In addition to [18], real-time measurements of PDL impairments in the presence of PMD were reported in [32], where a seven-stage emulator generating random "all-order" PMD and PDL states and a 112 Gb/s FPGA-based receiver were used. The Q-factors were measured with 31 ps mean PMD and with 1.3 dB mean PDL separately, as well as with combined PMD and PDL. However, the experiment did not include fiber transmission, and OSNR penalties were not measured.

In order to measure the tolerance of the 100G MSA transceiver to the combined effects of distributed PMD and PDL in a coherent long-haul transmission system, we again utilized the setup shown in Fig. 2. In this set of measurements, the remaining mid-stage attenuators were replaced by first-order fixed PDL elements, as listed in Table I. (We were limited to two PDL elements by equipment availability.) A measurement procedure similar to that described in Subsection V.A was used. Eight different runs of the experiment were performed, wherein several different combinations of DGD and instantaneous PDL thresholds (e.g., 50 ps DGD or 4.5 dB PDL) were used to access a wide range of DGDs and PDLs. A total of 3437 states were generated, of which 373 states had sufficiently large DGD or PDL for BER measurement. The launch state of polarization was fixed (i.e., not scrambled) and random relative to the PMD and PDL vectors. To our knowledge, these are the first such measurements of a 100 Gb/s coherent transceiver's tolerance to random, distributed PMD and PDL in a long-haul system to be reported in the literature.

Figure 12 displays the measured additional OSNR penalty to PMD and PDL versus the measured PDL (average of the PDL measured before and after the BER measurements) for these 373 states. Here, the "additional" OSNR penalty is defined as the difference between the required OSNR (at 1.9×10^{-2} pre-FEC BER) for the 10 × 100 km system with PMD and PDL and the 12.5 dB required OSNR for the system without PMD and PDL. There is a clear dependence of the OSNR penalty on PDL. For completeness, the results from the measurements of Subsection V.A (i.e., for 10 × 100 km with only PMD elements at the EDFA mid-stages) are also shown in Fig. 12. Separate measurements of the 100G MSA transceiver's tolerance to PDL from a variable first-order PDL element were also made, where the input polarization was scrambled slowly relative to the FEC frame. The black curve

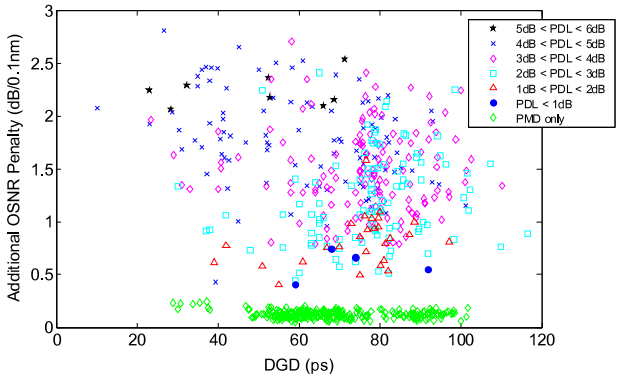

Fig. 13. (Color online) Measured additional OSNR penalties (defined in the text) versus DGD for the 10 × 100 km systems with PMD and PDL elements (various markers, sorted by the PDL) and with PMD elements only (green diamonds).

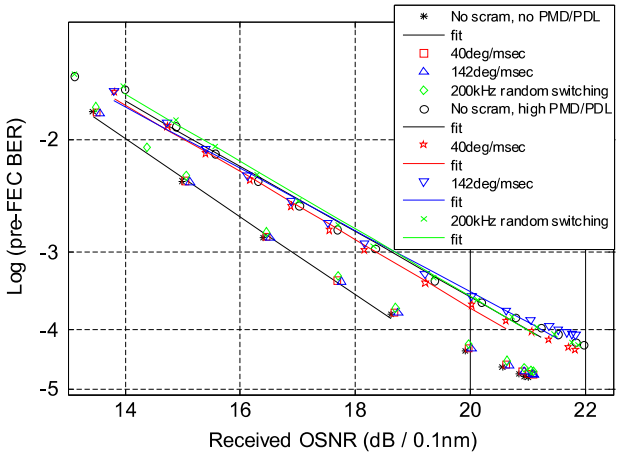

Fig. 14. (Color online) Measured pre-FEC BER versus OSNR, with and without polarization launch scrambling or switching, after transmission over 10 × 100 km without (first set of four curves with markers) and with the inter-stage PMD and PDL elements (second set of four curves with markers).

shown in Fig. 12 is the difference in required OSNR to have no uncorrectable FEC blocks with and without PDL. It therefore represents the penalty for the worst-case launch polarization with first-order PDL only. The results after 10 × 100 km with PMD and PDL follow the same trend as the PDL-only curve, where the spread in the OSNR penalties is due in part to the random launch polarization for each PMD/PDL state. Note that the transmission experiment includes higher-order PDL, which also contributes to the differences between the penalties after transmission and the PDL-only curve. When the required OSNRs for the 373 random PMD/PDL states are sorted by the measured PDL and plotted versus DGD, as shown in Fig. 13, it is clear that PDL, not PMD, is the dominant cause of the OSNR penalties, where penalties larger than 1 dB occur for PDLs greater than 2 dB.

C. Polarization Transients

An additional phenomenon that can occur in optical transmission systems is rapid change of the polarization state due to vibrations, activity of craft personnel, wind (if aerial cable) and other environmental factors. In coherent systems with polarization-multiplexed signals, the orientation of the polarization tributaries relative to the receiver polarization splitter is not controlled; thus the signal incident on the photodetectors after the hybrid is an arbitrary mixture of the two orthogonal transmitted polarization states. The coherent receiver recovers the signals on the two polarization tributaries using 4 × 4 multiple-input multiple-output equalization circuitry that tracks polarization and also compensates for PMD. Therefore, polarization transients define the maximum speed required of the polarization tracking implemented by the DSP. Previously, a real-time 40G coherent transceiver demonstrated tolerance to continuous scrambling of the input polarization at 570 deg/s after 8 × 100 km transmission [33] and to fast polarization transients (due to controlled mechanical shocks) with frequency content extending beyond 60 kHz [34].

Using the setup of Fig. 2, we measured the performance of the 100G MSA transceiver when the input polarization launch to the 10 × 100 km system was scrambled at various speeds using the N7788B polarization controller. BER versus received OSNR curves were measured with continuous scrambling speeds of 0 deg/ms, 40 deg/ms (based on [33]) and 142 deg/ms (the maximum speed of the N7788B polarization controller), along with a polarization switching speed of 200 kHz, where the launch polarization was switched to random states at a 200 kHz rate. Figure 14 shows eight BER curves, where the first four curves indicated by markers are for the 10 × 100 km system without the inter-stage PMD/PDL elements. The measurements with launch polarization scrambling and switching are nearly indistinguishable from the curve with no launch scrambling. For the second set of four curves, the 10 × 100 km system included the inter-stage PMD/PDL elements and had average DGD of 85 ps and average PDL of 3 dB (over the time required to make the BER measurements). The required OSNR for a pre-FEC BER of 1.9×10^{-2} had a spread of <0.4 dB for these four curves. These results indicate that the 100G MSA transceiver is tolerant to fast polarization transients.

VI. Ultra-Long-Haul Transmission With Accumulated Dispersion in Excess of 60,000 ps/nm

To explore the 100G MSA transceiver's performance in an ultra-long-haul transmission system, the two commercial systems A and B were cascaded, as shown in Fig. 6. We first explored the margin and the SD-FEC limit for system A by setting the 40G channels and 100G channel at their optimum launch powers (−2 dBm/ch and 0 dBm/ch, respectively, from Subsection III.B) and loading the 100G channel with ASE noise in front of the receiver. It was not possible to directly measure the OSNR at the receiver with conventional methods, due to ASE filtering at every ROADM and the fact that, if a channel is turned off at the transmit side, the commercial WDM system's control loops change the WSSs in all ROADMs to the block state for that channel. Therefore, the 100G PM-QPSK signal from the 100G transponder was replaced with a polarized,

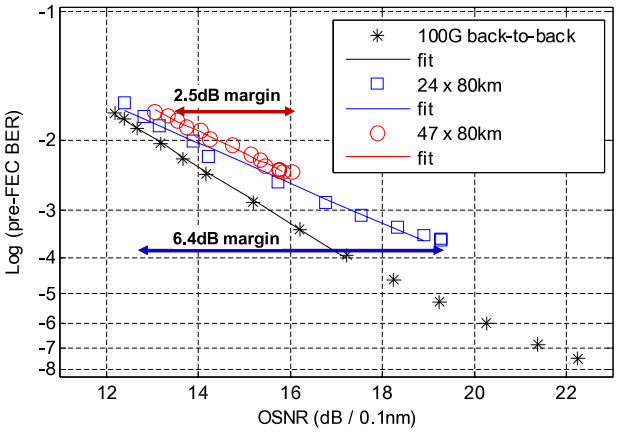

Fig. 15. (Color online) Measured pre-FEC BER versus OSNR after transmission over system A (24 × 80 km) and the cascade of systems A and B (47 × 80 km).

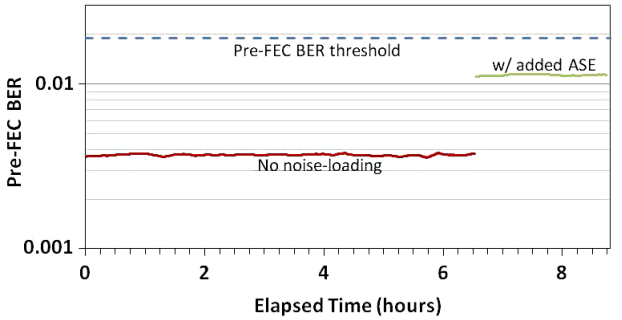

Fig. 16. (Color online) Measured line-side pre-FEC BER after 47 × 80 km transmission without (red curve) and with additional noise loading at the receiver (green curve). Zero errors were recorded on the 100G client-side test set during the soak tests.

continuous-wave signal at the same wavelength and power, and the received OSNR was estimated using the polarization nulling technique [35].

From our measurements, the OSNR for the 100G channel after the 1920 km link was about 19.2 dB for the optimized condition. With ASE noise loading after transmission, we did not observe any post-FEC errors until the OSNR was as low as 13 dB and the pre-FEC BER was over 1.7×10^{-2}, which is less than 0.18 dBQ from the FEC threshold and could be attributed to minor link and transponder control loop variations. The curve of pre-FEC BER versus received OSNR for the 1920 km link is shown in Fig. 15, along with the back-to-back curve for comparison. The results indicate that the transmission penalty is quite small; the penalty is about 0.6 dB at the pre-FEC BER of 1.7×10^{-2}. Based on the data in Fig. 15, the OSNR margin for the 100G transmission over 1920 km with SD-FEC is more than 6 dB.

Based on the available margin after 1920 km, the 100G channel was then transmitted through system B, comprised of 23 fiber spans and five additional ROADMs. As shown in Fig. 6(b), the 100G channel and 38 (100-GHz-spaced) 40G PM-QPSK channels were added at ROADM6, expressed through the next three ROADMs, and dropped at ROADM10, where the 100G channel was received. Figure 6(d) shows the optical spectrum at the input to system B, where the 39 channels were launched with 0 dBm/ch into the fiber spans. After 47 × 80 km transmission, the pre-FEC BER and OSNR for the 100G channel were 3.7×10^{-3} and about 16.0 dB, respectively, where again the received OSNR was measured using polarization nulling. The DSP in the coherent transceiver aptly compensated the total chromatic dispersion of the 3760 km link, which is in excess of 60,000 ps/nm and well beyond the specification of 50,000 ps/nm for the 100G transceiver and a recent report of 56,200 ps/nm compensation [36]. We added ASE noise to the 100G channel before the receiver and observed that, again, the 100G transponder did not show any post-FEC errors until the pre-FEC BER was over 1.7×10^{-2}. As shown in Fig. 15, the fiber transmission penalty for the 100G over 3760 km transmission is only about 1.2 dB at a pre-FEC BER of 1.7×10^{-2}. In addition, Fig. 15 shows that, with SD-FEC, the 100G channel still has 2.5 dB OSNR margin left after 3760 km transmission. On the other hand, if hard-coded FEC (with a pre-FEC BER threshold of 3.8×10^{-3}) is used, zero margin would be left after 3760 km, as shown by the BER at 16.0 dB OSNR in Fig. 15.

Finally, to verify the robustness of the 100G 47 × 80 km transmission, we performed soak tests and monitored the 100G performance after 3760 km using a client-side test set running in OTU4 mode (see client-side connections in Fig. 8). A soak over 6 hours without additional ASE noise loading (pre-FEC BER at 3.8×10^{-3}) was performed. Moreover, a second soak over 2 hours included additional noise loading to increase the pre-FEC BER to 1.2×10^{-2}, near the SD-FEC threshold, where a 0.6 dBQ margin was allowed for OSNR variation due to optical control loop fluctuations. (The total soak duration was limited by the standard work day.) Figure 16 shows the stability of the pre-FEC BER over the two soak tests, during which zero errors were recorded on the external 100G test set. These results indicate that the 100G MSA transceiver with SD-FEC is robust and capable of ultra-long-haul transmission with neighboring 40G channels and accumulated dispersion of more than 60,000 ps/nm.

VII. Conclusion

We have measured the performance of an industry-first real-time 120 Gb/s coherent transceiver module with integrated analog-to-digital conversion, DSP, and TPC-based soft-decision forward-error-correction coding. Through system experiments over 1000 km and longer distances, we demonstrated its high tolerance to various linear and nonlinear system impairments. The transceiver showed tolerance to a range of launch powers in long-haul DWDM systems with 40G and 100G neighboring channels and exhibited less than 1 dB penalty for MPI as high as −15 dBc. The transceiver was also measured to have high tolerance to polarization effects, including all-order PMD with up to 100 ps instantaneous DGD, polarization transients with switching speeds up to 200 kHz applied at the system input, and PDL, where less than 1 dB additional OSNR penalty was measured for PDLs up to 2 dB after 1000 km transmission.

In addition, we demonstrated the successful 3760 km transmission of the 100G MSA transceiver over commercial, uncompensated 40G-optimized DWDM ROADM systems with 80 km SSMF spans and 40G neighboring channels. Error-free transmission was verified on the client side with an external test set, and the transceiver had 2.5 dB OSNR margin after transmission and compensation of 60,000 ps/nm of chromatic dispersion. Our results validate that SD-FEC for 100G transmission is robust and that additional margin provided by SD-FEC over hard-coded FEC enables the 100G channels to be transmitted as far as, or even farther than, 40G channels.

ACKNOWLEDGMENTS

The authors would like to acknowledge T. Scherer, T. Downs and W. Keil of Nokia Siemens Networks for their assistance, and P. Magill of AT&T Labs—Research for his support of this work.

REFERENCES

[1] C. R. S. Fludger, T. Duthel, D. van den Borne, C. Schulien, E.-D. Schmidt, T. Wuth, E. de Man, G. D. Khoe, and H. de Waardt, "10 × 111 Gbit/s, 50 GHz spaced, POLMUX-RZ-DQPSK transmission over 2375 km employing coherent equalization," in *Proc. OFC*, Anaheim, CA, 2007, PDP22.

[2] C. R. S Fludger, T. Duthel, D. van den Borne, C. Schulien, E.-D. Schmidt, T. Wuth, J. Geyer, E. de Man, G. D. Khoe, and H. de Waardt, "Coherent equalization and POLMUX-RZ-DQPSK for robust 100-GE transmission," *J. Lightwave Technol.*, vol. 26, no. 1, pp. 64–72, Jan. 2008.

[3] P. Winzer, "Beyond 100G Ethernet," *IEEE Commun. Mag.*, vol. 48, no. 7, pp. 26–30, July 2010.

[4] F. Chang, K. Onohara, and T. Mizuochi, "Forward error correction for 100G transport networks," *IEEE Commun. Mag.*, vol. 48, no. 3, pp. S48–S55, 2010.

[5] O. Ait Sab, "FEC techniques in submarine transmission systems," in *Proc. OFC/NFOEC*, Anaheim, CA, 2001, TuF1.

[6] M. Akita, H. Fujita, T. Mizuochi, K. Kubo, H. Yoshida, K. Kuno, and S. Kurahashi, "Third generation FEC employing Turbo Product Code for long-haul DWDM transmission systems," in *Proc. OFC/NFOEC*, Anaheim, CA, 2002, WP2.

[7] Y. Miyata, K. Sugihara, W. Matsumoto, K. Onohara, T. Sugihara, K. Kubo, H. Yoshida, and T. Mizuochi, "A triple-concatenated FEC using soft-decision decoding for 100 Gb/s optical transmission," in *Proc. OFC/NFOEC*, San Diego, CA, 2010, OThL3.

[8] K. Onohara, T. Sugihara, Y. Konishi, Y. Miyata, T. Inoue, S. Kametani, K. Sugihara, K. Kubo, H. Yoshida, and T. Mizuochi, "Soft-decision-based forward error correction for 100 Gb/s transport systems," *IEEE J. Sel. Top. Quantum. Electron.*, vol. 16, no. 5, pp. 1258–1267, Sept./Oct. 2010.

[9] L. E. Nelson, Y. Pan, M. Birk, R. Isaac, C. Rasmussen, M. Givehchi, and B. Mikkelsen, "WDM performance and multiple-path interference tolerance of a real-time 120 Gbps Pol-Mux QPSK transceiver with soft decision FEC," in *Proc. NFOEC*, Los Angeles, CA, 2012, NTh1I.5.

[10] G. Zhang, L. E. Nelson, Y. Pan, M. Birk, C. Skolnick, C. Rasmussen, M. Givehchi, B. Mikkelsen, T. Scherer, T. Downs, and W. Keil, "3760 km, 100G SSMF transmission over commercial terrestrial DWDM ROADM systems using SD-FEC," in *Proc. OFC/NFOEC*, Los Angeles, CA, 2012, PDP5D.4.

[11] B. Spinnler, "Recent advances on polarization multiplexing," in *Proc. LEOS Summer Topical Meeting*, Acapulco, Mexico, 2008, TuD2.3.

[12] S. Savory, "Digital coherent optical receivers: algorithms and subsystems," *IEEE J. Sel. Top. Quantum Electron.*, vol. 16, no. 5, pp. 1164–1179, Sept./Oct. 2010.

[13] J. Bromage, L. E. Nelson, C. H. Kim, P. J. Winzer, R.-J. Essiambre, and R. M. Jopson, "Relative impact of multiple-path interference and amplified spontaneous emission noise on optical receiver performance," in *Proc. OFC/NFOEC*, Anaheim, CA, 2002, TuR3.

[14] C. Martinelli, G. Charlet, L. Pierre, J. Antona, and D. Bayart, "System impairment of double-Rayleigh scattering and dependence on modulation format," in *Proc. OFC/NFOEC*, Atlanta, Georgia, 2003, FE3.

[15] C. R. S. Fludger, Y. Zhu, V. Handerek, and R. J. Mears, "Impact of MPI and modulation format on transmission systems employing distributed Raman amplification," *Electron. Lett.*, vol. 37, no. 15, pp. 970–972, July 19, 2001.

[16] L. E. Nelson, X. Zhou, S. L. Woodward, S. Foo, H. Sun, M. Moyer, and M. O'Sullivan, "Tolerance of 46-Gb/s dual-polarization quadrature-phase shift keyed signals to multiple-path interference," in *Proc. OFC/NFOEC*, San Diego, CA, 2009, OTuN3.

[17] A. Klekamp and H. Bülow, "Experimental comparison of PMD tolerances of binary 43 Gb/s modulation formats without and with PMD compensation," in *Proc. ECOC*, Cannes, France, 2006, Tu4.2.4.

[18] H. Sun, K.-T. Wu, and K. Roberts, "Real-time measurements of a 40 Gb/s coherent system," *Opt. Express*, vol. 16, no. 2, pp. 873–879, Jan. 21, 2008.

[19] L. E. Nelson, S. L. Woodward, S. Foo, X. Zhou, M. D. Feuer, D. Hanson, D. McGhan, H. Sun, M. Moyer, M. O. Sullivan, and P. D. Magill, "Performance of a 46-Gbps dual-polarization QPSK transceiver with real-time coherent equalization over high PMD fiber," *J. Lightwave Technol.*, vol. 27, no. 3, pp. 158–169, Feb. 2009.

[20] C. Xie, "Polarization-mode-dispersion impairments in 112- Gb/s PDM-QPSK coherent systems," in *Proc. ECOC*, Torino, Italy, 2010, Th.10.E.6.

[21] L. E. Nelson and S. L. Woodward, "Capabilities of real-time digital coherent transceivers," in *Proc. ECOC*, Torino, Italy, 2010, Mo.1.C.5.

[22] M. Birk, P. Gerard, R. Curto, L. E. Nelson, X. Zhou, P. Magill, T. J. Schmidt, C. Malouin, B. Zhang, E. Ibragimov, S. Khatana, M. Glavanovic, R. Lofland, R. Marcoccia, R. Saunders, G. Nicholl, M. Nowell, and F. Forghieri, "Real-time single-carrier coherent 100 Gb/s PM-QPSK field trial," *J. Lightwave Technol.*, vol. 29, no. 4, pp. 417–425, Feb. 2011.

[23] R. M. Craig, "Visualizing the limitations of four-state measurement of PDL and results of a six-state alternative," in *Symp. on Optical Fiber Measurements (SOFM 2002)*, Boulder, CO, Sept. 24–26, 2002, pp. 121–124.

[24] R. M. Jopson, L. E. Nelson, and H. Kogelnik, "Measurement of second-order polarization-mode dispersion vectors in optical fibers," *IEEE Photon. Technol. Lett.*, vol. 11, no. 9, pp. 1153–1155, Sept. 1999.

[25] B. Heffner, "Automated measurement of polarization mode dispersion using Jones matrix eigenanalysis," *IEEE Photon. Technol. Lett.*, vol. 4, no. 9, pp. 1066–1069, Sept. 1992.

[26] S. L. Woodward, L. E. Nelson, M. D. Feuer, X. Zhou, P. D. Magill, S. Foo, D. Hanson, D. McGhan, H. Sun, M. Moyer, and M. O'Sullivan, "Characterization of real-time PMD and chromatic dispersion monitoring in a high-PMD 46-Gbps transmission system," *IEEE Photon. Technol. Lett.*, vol. 20, no. 24, pp. 2048–2050, Dec. 2008, and references therein.

[27] S. L. Woodward, L. E. Nelson, C. R. Schneider, L. A. Knox, M. O'Sullivan, C. Laperle, M. Moyer, and S. H. Foo, "Field observations of optical parameters using integrated performance monitoring," in *Proc. OFC/NFOEC*, Los Angeles, CA, 2012, JWA20.

[28] T. Duthel, C. R. S. Fludger, J. Geyer, and C. Schulien, "Impact of polarization dependent loss on coherent POLMUX-NRZ-DQPSK," in *Proc. OFC/NFOEC*, San Diego, CA, 2008, OThU5.

[29] O. Vassilieva, T. Hoshida, X. Wang, J. Rasmussen, H. Miyata, and T. Naito, "Impact of polarization dependent loss and cross-phase modulation on polarization multiplexed DQPSK signals," in *Proc. OFC/NFOEC*, San Diego, CA, 2008, OThU6.

[30] C. Xie, "Polarization-dependent loss induced penalties in PDM-QPSK coherent optical communication systems," in *Proc. OFC/NFOEC*, San Diego, CA, 2010, OWE6.

[31] M. Shtaif, "Performance degradation in coherent polarization multiplexed systems as a result of polarization dependent loss," *Opt. Express*, vol. 16, no. 18, pp. 13918–13932, Sept. 2008.

[32] T. Tanimura, Y. Aoki, H. Nakashima, T. Hoshida, J. Li, Z. Tao, and J. C. Rasmussen, "FPGA-based 112 Gb/s coherent DP-QPSK receiver and multi-stage PMD-PDL emulator for fast evaluation of digital signal processing algorithms," in *Proc. ECOC*, Torino, Italy, 2010, Tu.5.A.3.

[33] L. E. Nelson, "Polarization effects in coherent systems," in *Proc. OFC/NFOEC*, Los Angeles, CA, 2012, OTu1A.4.

[34] K. Roberts, M. O'Sullivan, K.-T. Wu, H. Sun, A. Awadalla, D. J. Krause, and C. Laperle, "Performance of dual-polarization QPSK for optical transport systems," *J. Lightwave Technol.*, vol. 27, no. 16, pp. 3546–3559, Aug. 2009.

[35] M. Rasztovits-Wiech, M. Danner, and W. R. Leeb, "Optical signal-to-noise-ratio measurement in WDM networks using polarization extinction," in *Proc. ECOC*, Sept. 1998, pp. 549–550.

[36] M. Arikawa, T. Okamoto, E. de Gabory, T. Ito, and K. Fukuchi, "WDM transmission of 127 Gb/s PM-QPSK signal over 3350 km SMF-only line with chromatic dispersion compensation using real-time DSP-LSI," in *Proc. OFC/NFOEC*, Los Angeles, CA, 2012, NTh1I.4.